

Holographic study of shear viscosity and butterfly velocity for magnetic field-driven quantum criticality

Jun-Kun Zhao^{a1} and Li Li^{a,b,c2}

^a*CAS Key Laboratory of Theoretical Physics, Institute of Theoretical Physics, Chinese Academy of Sciences, Beijing 100190, China*

^b*School of Physical Sciences, University of Chinese Academy of Sciences, No.19A Yuquan Road, Beijing 100049, China*

^c*School of Fundamental Physics and Mathematical Sciences, Hangzhou Institute for Advanced Study, UCAS, Hangzhou 310024, China*

Abstract

We investigate the shear viscosity and butterfly velocity of a magnetic field-induced quantum phase transition in five dimensional Einstein-Maxwell-Chern-Simons theory, which is holographically dual to a class of strongly coupled quantum field theories with chiral anomalies. Our analysis reveals that the ratio of longitudinal shear viscosity to entropy density η_{\parallel}/s exhibits a pronounced non-monotonic dependence on temperature T when the magnetic field B is slightly below the critical value B_c of the quantum phase transition. In particular, it can develop a distinct minimum at an intermediate temperature. This contrasts sharply with the monotonic temperature scaling observed at and above B_c , where η_{\parallel}/s follows the scaling $T^{2/3}$ at $B = B_c$ and transitions to T^2 for $B > B_c$ as $T \rightarrow 0$. The non-vanishing of η_{\parallel}/s for $B < B_c$ in the zero temperature limit suggests that it could serve as a good order parameter of the quantum phase transition. We also find that all butterfly velocities change dramatically near the quantum phase transition, and thus their derivatives with respect to B can be independently used to detect the quantum critical point.

¹Email: junkunzhao@itp.ac.cn

²Email: liliphy@itp.ac.cn

Contents

1	Introduction	1
2	Holographic setup	4
2.1	Quantum criticality	5
3	Shear viscosity	7
4	Butterfly velocity	12
4.1	Butterfly velocity from shock wave geometry	12
4.2	Butterfly velocity from pole-skipping	14
4.3	Relation between shear viscosity and butterfly velocity	17
5	Conclusion and discussion	18
A	Holographic renormalization	20
B	Transverse shear viscosity	23
C	Longitudinal shear viscosity for $k = 0$	24

1 Introduction

Quantum phase transition (QPT), driven by quantum fluctuations at absolute zero temperature, plays a crucial role in understanding exotic properties of strongly-correlated quantum matter [1]. Specifically, the quantum critical point (QCP) can dominate a broad regime of the phase diagram away from it, offering valuable insights into the mysteries, for example, in high-temperature superconductors and strange metals. Moreover, the dynamics near the QCP may go beyond the traditional framework of the Landau-Ginzburg-Wilson paradigm [2–5]. A hallmark of quantum criticality is the emergence of scale invariance at the QCP, where the system could be governed by conformal field theory (CFT). This suggests a profound connection to the Anti-de Sitter/Conformal Field Theory (AdS/CFT) correspondence [6], particularly when the CFT possesses a large central charge. Indeed, holographic techniques have been applied to describe strongly coupled quantum critical systems without quasi-particles, providing a non-perturbative

and readily accessible approach for investigating various transports as well as the far-from-equilibrium dynamics [7–9]. In holography, significant progress has been made in modeling QPTs in dual strongly coupled many-body systems (see *e.g.* [10–14]). Among them, the most intriguing one is the QPT driven by a magnetic field, which occurs without symmetry breaking and is described by the Einstein-Maxwell-Chern-Simons theory (EMCS) [11].

The five dimensional EMCS theory is one of the benchmark models in AdS/CFT, which is dual to a class of strongly coupled systems with chiral anomaly [15]. It offers a robust testing ground in the construction of chiral hydrodynamic constitutive relations with magnetic field [16] and the study of anomalous hydrodynamics effective action [17]. In this theory, the interplay between finite charge density and magnetic field yields a strongly coupled anisotropic system with a magnetic field induced QPT [11, 18–20]. Although it has received a lot of interest [21–24], the physical interpretation of this phenomenon remains obscure due to the lack of a good order parameter, and more properties associated with quantum criticality are still undiscovered. Therefore, it is necessary to study it from multiple perspectives. In the present work, we aim at probing the quantum criticality of the QPT by using shear viscosity and butterfly velocity. We note that the shear viscosity in this holographic model was initially computed in [16], working at a relatively high temperature and strong magnetic field. Some properties of butterfly velocities were considered in [25, 26], which suggested that one must employ at least two butterfly velocities to identify the location of the QCP. Despite this, the fundamental impacts of QPT on shear viscosity and butterfly velocity remain largely unexplored. This motivates us to revisit the question of the properties of shear viscosity and butterfly velocity, focusing on the effects of quantum criticality.

One of the most quantitative applications of holography to strongly correlated systems is the ratio of shear viscosity to entropy density $\eta/s = \hbar/(4\pi k_B)$ that is universal in a large class of theories, known as the Kovtun-Son-Starinets (KSS) bound [27, 28]. Nevertheless, there are some ways for which the KSS bound could be violated. Firstly, certain higher derivative corrections to the low-energy Einstein action can push η/s below the KSS bound, while causality constraints in the boundary theory impose a revised lower bound [29–31]³. Second, within Einstein gravity, violations were realized by breaking spacetime symmetries (translations and/or rotations) [38–45]. However, the breaking of rotations itself does not necessarily imply a violation of the KSS bound [46, 47]. Moreover, KSS bound can be violated in far-from-equilibrium processes [48–50]. Another crucial aspect involves the construction of holographic models in which η/s exhibits a temperature-dependent behavior, reaching a characteristic minimum at the phase

³For more research on higher derivative corrections, one can refer to, for instance, [32–36]. Additionally, a comprehensive review can be found in [37].

transition—a phenomenon observed for various fluids in nature. However, only a limited number of holographic models that incorporate higher-derivative corrections display a non-monotonic temperature dependence η/s [51, 52] where the effects are perturbatively small.

On the other hand, it has been revealed that there is an inextricable connection between late-time hydrodynamic transports and early-time chaotic properties in quantum many-body systems [53–56]. It is well-known that chaos is a fundamental property inherent in thermal systems, manifesting universally across a wide range of physical phenomena. In quantum many-body systems, chaotic dynamics can be rigorously characterized through the exponential growth of the out-of-time-order correlator (OTOC). In a large class of many-body systems, it has been observed that [57–61]

$$\langle V(t, \vec{x}) W(0) V(t, \vec{x}) W(0) \rangle_\beta = 1 - \epsilon e^{\lambda \left(t - \frac{|\vec{x}|}{v_B} \right)} + \dots, \quad (1.1)$$

where V and W denote generic local few-body operators, $\beta = 1/T$ represents the inverse temperature, and $\epsilon \sim \mathcal{N}^{-1}$ parameterizes the degrees of freedom \mathcal{N} of the system. Furthermore, λ corresponds to the quantum Lyapunov exponent that is bounded by $\lambda \leq 2\pi\beta$ [60], and v_B is the butterfly velocity characterizing information scrambling in spatial dimensions. For strongly coupled quantum matter with gravity dual, the quantum chaos can be determined from the two sided eternal black hole dual to the thermofield double state of two identical CFTs L and R [58, 59]. Remarkably, the pole-skipping phenomenon clearly demonstrates the connection between quantum chaos and hydrodynamic transports with λ and v_B being identified at the pole-skipping point [56, 62, 63].

In this paper, we study the shear viscosity within the framework of EMCS theory exhibiting a magnetic field-driven QPT. The presence of magnetic field breaks the spatial $SO(3)$ rotational symmetry into $SO(2)$ symmetry in the plane orthogonal to the magnetic field. Consequently, there is one universal transverse shear viscosity η_\perp , one non-universal longitudinal shear viscosity η_\parallel , as well as two Hall viscosities. The expression for transverse shear viscosity can be derived analytically and equals the famous KSS value with $\eta_\perp/s = 1/4\pi$ (hereafter $\hbar = k_B = 1$). Nevertheless, because of the non-zero Chern-Simons (CS) coupling, an analytical expression for the longitudinal shear viscosity is not currently accessible. Therefore, the η_\parallel are computed numerically using the pseudo-spectrum method. Our findings reveal that the ratio η_\parallel/s could exhibit non-monotonic behavior with respect to the magnetic field or temperature. In some cases, the ratio η_\parallel/s decreases and then increases with respect to temperature, resulting in a distinct minimum at an intermediate temperature. This feature demonstrates a striking similarity to what is observed in most fluids, thereby paving the way for the construction of holographic models for strongly coupled fluids, such as quark-gluon plasma. Furthermore, at extremely low temperatures, the ratio η_\parallel/s is finite for $B < B_c$ but approaches

zero for $B > B_c$, suggesting its potential role as a useful order parameter for the QPT in present theory. On the other hand, the butterfly velocity has been computed using two independent methods: the shock wave analysis and the pole-skipping phenomenon. Both methods yield consistent results and correctly reproduce the splitting of butterfly velocities in the direction parallel to the magnetic field. Moreover, our study shows that each butterfly velocity displays an abrupt change across the QPT, demonstrating its ability to pinpoint the location of QCP through its derivative with respect to the magnetic field, *i.e.* $\partial v_B / \partial B$. We also investigate the relation between shear viscosity and butterfly velocity.

The paper is organized as follows. In Section 2 we introduce the holographic model that exhibits the magnetic field-induced QPT. We study the behaviors of shear viscosity and butterfly velocity of the system in Section 3 and Section 4, respectively. We conclude and discuss the open questions in Section 5. More technical details are provided in the appendices.

2 Holographic setup

We consider the five dimensional EMCS theory that is derived from a consistent truncation of Type IIB supergravity or M-theory [64, 65].

$$S = \frac{1}{16\pi G_N} \int d^5x \sqrt{-g} \left(R + \frac{12}{L^2} - \frac{1}{4} F_{ab} F^{ab} + \frac{k}{24} \epsilon^{abcde} A_a F_{bc} F_{de} \right), \quad (2.1)$$

where the Maxwell field strength $F_{ab} = \partial_a A_b - \partial_b A_a$. Here G_N is Newton's constant, L is the AdS radius, and $k = \frac{2}{\sqrt{3}}$ is the CS coupling.⁴ The corresponding equations of motion read

$$G_{ab} - 6g_{ab} - \frac{1}{2} \left(F_{ac} F_b{}^c - \frac{1}{4} g_{ab} F_{cd} F^{cd} \right) = 0, \quad (2.2)$$

$$\nabla_b F^{ba} + \frac{k}{8} \epsilon^{abcde} F_{bc} F_{de} = 0, \quad (2.3)$$

where we have set $16\pi G_N = 1$ and $L = 1$, without loss of generality.

To study the magnetic field-driven QPT, we consider the following dyonic black brane solution [11, 22]:

$$ds^2 = \frac{1}{r^2} \left[- (f - h^2 p^2) dt^2 + 2ph^2 dt dz + g(dx^2 + dy^2) + h^2 dz^2 + \frac{dr^2}{f} \right], \quad (2.4)$$

$$A = A_t dt - \frac{B}{2} y dx + \frac{B}{2} x dy - A_z dz,$$

⁴From the bottom-up point of view, the CS coupling k can be treated as a free parameter. For $k > k_c \approx 1.158$, this system is known to be unstable below a critical temperature towards the formation of a helical order [66, 67].

where f, g, h, p, A_t and A_z are functions of the holographic coordinate r . The system approaches the asymptotically AdS boundary as $r \rightarrow 0$, while it goes to the event horizon when $r \rightarrow r_h$. The temperature and entropy density of the system read

$$T = -\frac{f'(r)}{4\pi}\Big|_{r=r_h}, \quad s = \frac{4\pi g(r)h(r)}{r^3}\Big|_{r=r_h}. \quad (2.5)$$

Note that the magnetic field B breaks Lorentz invariance along the z -axis, leading to spatial anisotropy of the system.

After solving the bulk equations of motion, we can extract thermodynamic quantities, such as the free energy density, chemical potential and energy density. We point out that the CS term results in a non-trivial correction to the thermodynamics of the above dyonic black brane. In particular, the free energy density derived through the quantum statistical relation violates the standard form of the first law of thermodynamics. This issue has been addressed in our recent work [24] (see also Appendix A for more details). We shall work in the grand canonical ensemble by fixing the chemical potential $\mu = 1$.

2.1 Quantum criticality

We now turn to the quantum criticality associated with the QPT induced by the magnetic field. When $B = 0$, the system can be solved analytically and the solution is known as the electrically charged Reissner-Nordström (RN) black brane.

$$f = 1 - \left(1 + \frac{\mu^2 r_h^2}{3}\right) \frac{r^4}{r_h^4} + \frac{\mu^2}{3r_h^4} r^6, \quad A_t = \mu \left(1 - \frac{r}{r_h}\right)^2, \quad (2.6)$$

with $g = h = 1, p = A_z = 0$. As $T \rightarrow 0$, the near horizon geometry of the RN solution is $AdS_2 \times R^3$. On the other hand, for sufficiently strong magnetic field ($\vec{B} \propto \vec{z}$), the $x - y$ plane will stop to contract in the deep infrared region, resulting in $AdS_3 \times R^2$ near horizon geometry [18]. Consequently, the interplay between the charge density and the magnetic field will give rise to a QPT at the critical magnetic field $B_c \approx 0.332$ [11]. In this case, numerical methods are necessary to obtain the full solution, for which we will employ the spectral method to solve the equations of motion.

It has been established that scaling of entropy density near the QCP takes [11, 19]

$$s = T^{1/3} \phi_s \left(\frac{B - B_c}{T^{2/3}} \right), \quad (2.7)$$

where ϕ_s is a scaling function of the normalized magnetic field B and temperature T . Following the standard scaling hypothesis, one can deduce from (2.7) that the dynamical critical exponent $z = 3$ and the correlation length exponent $\nu = 1/2$. As a demonstration,

Figure 1 illustrates the temperature scaling of the entropy density at different phases. Above the quantum critical point *i.e.* at $B = B_c \approx 0.332$, the entropy density scales as $s \sim T^{1/3}$, which confirms the analytical result (2.7). When $B = 0.326 < B_c$, the entropy decreases to a constant in the extremal low temperature. In contrast, when $B = 0.338 > B_c$, the entropy displays a linear temperature dependence $s \sim T$ as $T \rightarrow 0$.

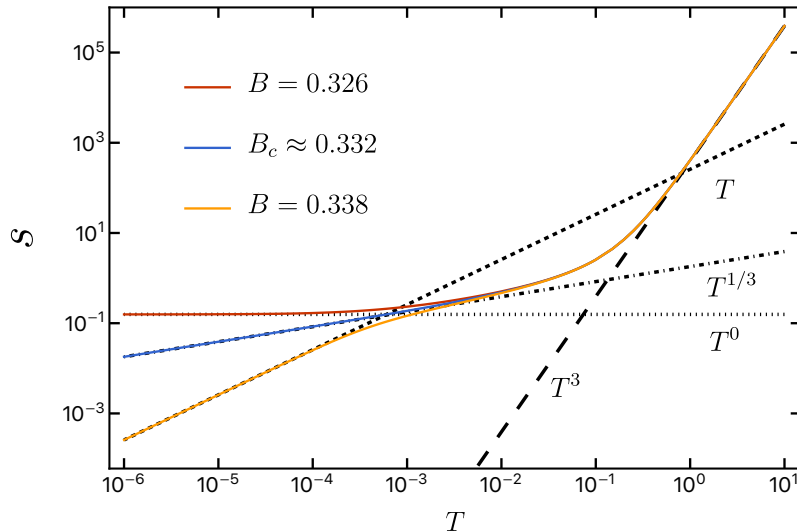


Figure 1: The entropy density s as a function of temperature T in different phases. There is a QPT at the critical magnetic field at $B_c \approx 0.332$. We consider $k = 2/\sqrt{3}$ and fix the chemical potential $\mu = 1$.

Within the Landau paradigm, phases of matter are characterized by their symmetries, and whether or not those are spontaneously broken which is associated with a local order parameter. The QPT defies the Landau paradigm as there is no symmetry breaking for all phases of (2.4). From the gravitational perspective, the mechanism driving this QPT can be interpreted as the expulsion of electric charge from the black hole horizon into the bulk, occurring as the magnetic field gradually increases from zero. This charge expulsion process terminates at a critical magnetic field strength $B = B_c$, where the black hole horizon becomes electrically neutral. Based on this charge expulsion mechanism, this QPT could be referred to as a transition from a “fractionalized” phase with charged horizons ($B < B_c$) to a “cohesive” phase with charged matter in the bulk ($B > B_c$) [20] (see also [12, 68]).

In the following part, we shall study the properties of shear viscosity and the butterfly velocity of the strongly coupled quantum many-body system dual to the EMCS theory. We are primarily concerned with how the presence of quantum criticality influences the behavior of shear viscosities and butterfly velocities.

3 Shear viscosity

The viscosity tensor can be defined via the Kubo formula as

$$\eta_{ij,kl} = \lim_{\omega \rightarrow 0} \frac{1}{\omega} \text{Im}[G_{ij,kl}^R(\omega, 0)], \quad (3.1)$$

where the retarded correlation for the energy-momentum tensor is given by

$$G_{ij,kl}^R(\omega, 0) = - \int dt d^3x e^{i\omega t} \theta(t) \langle [T_{ij}(t, \vec{x}), T_{kl}(0, 0)] \rangle, \quad (3.2)$$

evaluated at zero wave-vector $\vec{k} = 0$ and finite frequency ω . The above retarded Green functions are holographically dual to the metric fluctuations on the background solutions. Therefore, all we need is to solve the bulk equations of motion for metric fluctuations which could be, in principle, coupled with other perturbations.

In our system, the spatial $SO(3)$ rotation symmetry is broken explicitly due to the presence of background magnetic field, but fortunately a $SO(2)$ symmetry along the transverse direction is preserved. For this specific symmetry breaking, there exist two shear viscosities which are related to the symmetric part of $\eta_{ij,kl}$, *i.e.*

$$\eta_{\parallel} = \eta_{xz,xz} = \eta_{yz,yz}, \quad \eta_{\perp} = \eta_{xy,xy}. \quad (3.3)$$

Additionally, the presence of chiral anomaly contributes two more dissipationless Hall viscosities (antisymmetric part of $\eta_{ij,kl}$), *i.e.*

$$\eta_{H\parallel} = \eta_{yz,xz}, \quad \eta_{H\perp} = \eta_{xy,xx} = \eta_{xy,yy}, \quad (3.4)$$

and we will not consider the Hall viscosities in the present work.

To determine the transports of the system, we should consider fluctuations of g_{ab} and A_b above the background solution (2.4). The general form of the fluctuations takes

$$g_{ab} = \bar{g}_{ab} + \int d\omega d^3k e^{ik_{\mu}x^{\mu}} h_{ab}(r, k^{\mu}), \quad A_b = \bar{A}_b + \int d\omega d^3k e^{ik_{\mu}x^{\mu}} a_b(r, k^{\mu}), \quad (3.5)$$

where \bar{g}_{ab} and \bar{A}_b denote the background solutions, and $k^{\mu} = (\omega, \vec{k})$. By choosing the radial gauge $a_r = 0, h_{ra} = 0$, we can classify the physical fluctuations according to how they transfer under the $SO(2)$ along the (x, y) plane.⁵

One can show that the helicity two perturbation h_{xy} leads to the universal $\eta_{\perp}/s = 1/4\pi$ behavior, see Appendix B for more details. On the other hand, the modes from the helicity one sector are responsible for a non-universal shear viscosity η_{\parallel} . Therefore, in our analysis, we will focus exclusively on the helicity one sector.

⁵One can find that $\eta_{H\perp} = 0$ due to the decoupling between h_{xy} and $h_{xx} - h_{yy}$.

Helicity	Fluctuations
2	$h_{xy}, h_{xx} - h_{yy}$
1	$h_{tx}, h_{ty}, h_{xz}, h_{yz}, a_x, a_y$
0	$h_{tt}, h_{tz}, h_{zz}, h_{xx} + h_{yy}, a_t, a_z$

The computation of the non-universal shear viscosity is highly non-trivial, as these modes in the helicity one sector are all coupled to each other. It has been shown that for an anisotropic bulk system there could be an analytical horizon formula for the longitudinal shear viscosity, see *e.g.* [46]. Unfortunately, all known examples were found for the static case, while the present geometry (2.4) is not a static one due to the CS coupling. Therefore, we decide to obtain η_{\parallel} by solving the equations of motion numerically. For numerical convenience, we introduce

$$Y_{\pm} = h^x_z \pm ih^y_z, \quad Z_{\pm} = h^x_t \pm ih^y_t, \quad a_{\pm} = a_x \pm ia_y, \quad (3.6)$$

that can split the helicity one fluctuations into two decoupled sectors: (Y_+, Z_+, a_+) and (Y_-, Z_-, a_-) . Consequently, the simplified equations of motion for helicity one fluctuations can be written as

$$Y_{\pm}'' + R_1 Y_{\pm}' + \left(\frac{\omega^2}{f^2} - \frac{B^2 r^2}{fg^2} \right) Y_{\pm} + \frac{h^2 p'}{f} Z_{\pm}' - \frac{r^2 A'_z}{g} a'_{\pm} = 0, \quad (3.7)$$

$$Z_{\pm}'' + S_1 Z_{\pm}' - \frac{B^2 r^2}{fg^2} Z_{\pm} + S_2 Y_{\pm}' + \frac{\omega^2 p}{f^2} Y_{\pm} + \frac{r^2}{g} \left(A'_t a_{\pm} \mp \frac{\omega B}{fg} a_{\pm} \right) = 0, \quad (3.8)$$

$$a_{\pm}'' + T_1 a_{\pm}' + \left(\frac{\omega^2}{f^2} \mp \frac{k\omega r A'_z}{fh} \right) a_{\pm} + T_2 Z_{\pm}' + T_3 Y_{\pm}' - \frac{Bkr}{fh} (A'_z Z_{\pm} + A'_t Y_{\pm}) \pm \frac{\omega B}{f^2} (Z_{\pm} - pY_{\pm}) = 0, \quad (3.9)$$

together with the coefficients

$$\begin{aligned} R_1(r) &= \frac{f'}{f} + \frac{2g'}{g} - \frac{h'}{h} - \frac{h^2 pp'}{f} - \frac{3}{r}, \\ S_1(r) &= \frac{2g'}{g} + \frac{h'}{h} + \frac{h^2 pp'}{f} - \frac{3}{r}, \quad S_2(r) = p \left(\frac{f'}{f} - \frac{2h'}{h} \right) - p' - \frac{h^2 p^2 p'}{f}, \\ T_1(r) &= \frac{f'}{f} + \frac{h'}{h} - \frac{1}{r}, \quad T_2(r) = \frac{g}{f} (A'_t + pA'_z), \quad T_3(u) = \frac{gA'_z}{h^2} - pT_2(r). \end{aligned}$$

Since we are interested in the shear viscosity, we will only turn on the source term for Y_{\pm} , for which the equations can be solved numerically after imposing the ingoing boundary conditions at the event horizon $r = r_h$. The UV expansions for the fluctuations can be found in Appendix A.

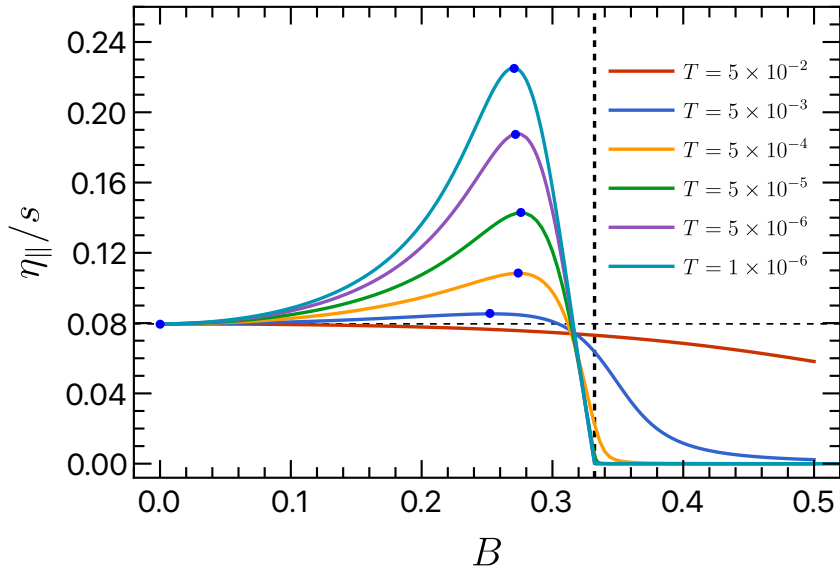


Figure 2: The ratio $\eta_{||}/s$ as a function of magnetic field at different temperatures. The blue point marks the maximum of each curve. The dashed horizontal line represents the KSS bound, while the dashed vertical line marks the location of QCP. We choose $k = 2/\sqrt{3}$ and $\mu = 1$.

The behavior of $\eta_{||}/s$ as a function of magnetic field at different temperatures is shown in Figure 2. In high temperature, starting from the KSS bound, the value of $\eta_{||}/s$ decreases monotonically to a small value as the strength of the magnetic field increases (see the red curve). Interestingly, at low temperatures, the ratio $\eta_{||}/s$ first increases to a maximum value $(\eta_{||}/s)_0$ at B_0 before the critical magnetic field B_c (vertical line) is reached and then decreases monotonically to an extremely small value when $B > B_c$ ⁶. The location of the peak $(B_0, (\eta_{||}/s)_0)$ that is marked by a blue point depends on the temperature.

In the left panel of Figure 3, we show the behavior of B_0 and $(\eta_{||}/s)_0$ with respect to temperature. While the value of B_0 (red curve) saturates at the low temperature limit, the maximum value of $\eta_{||}/s$ (blue curve) increases monotonically as the temperature decreases. For the temperature range we show, the maximum value of $\eta_{||}/s$ can be three times larger than the famous KSS value. In contrast, when $B > B_c$, the $\eta_{||}/s$ ratio generally vanishes at zero temperature following a universal power-law $\sim T^2$ consistent with the result of $\eta_{||}/s$ in purely magnetic black brane [41], see the right panel of Figure 3.

⁶The behavior of $\eta_{||}/s$ with respect to magnetic field was first studied in [16], yet working at a relative high temperature and strong magnetic field regime, *i.e.* for $0.08 < T/\mu < 4$ and $0 < B/\mu^2 < 18$. The non-monotonic magnetic field dependence of $\eta_{||}/s$ there is parametrically small, and the crucial role played by the quantum criticality has not been addressed. As shown in Figure 1, the quantum critical regime can only be touched at temperatures much lower than $T/\mu \sim 10^{-3}$.

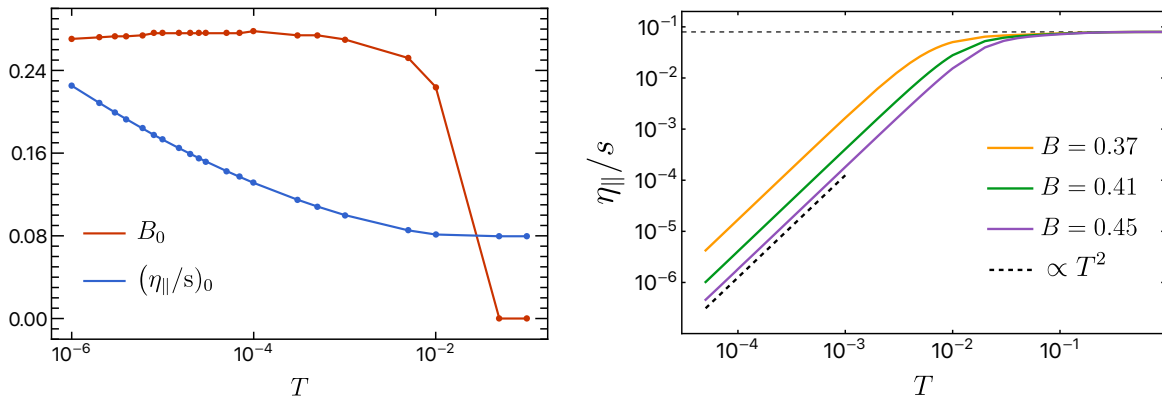


Figure 3: Left panel: The maximum $(B_0, (\eta_{\parallel}/s)_0)$ (blue points in Figure 2) as a functions of temperature. Right panel: The ratio η_{\parallel}/s as a function temperature for different $B > B_c$. The plots are generated for $k = 2/\sqrt{3}$ and $\mu = 1$.

Therefore, in the zero temperature limit $T \rightarrow 0$, we have

$$\eta_{\parallel}/s > 0 \quad (B < B_c), \quad \eta_{\parallel}/s = 0 \quad (B > B_c). \quad (3.10)$$

This suggests that the low temperature limit of η_{\parallel}/s could be a good order parameter for probing the QPT in the present system.⁷

Figure 4 shows the temperature dependence of the ratio η_{\parallel}/s in different magnetic fields. For small B , the ratio η_{\parallel}/s first decreases and then increases to a value much higher than the value of the KSS bound as we decrease the temperature, see *e.g.* the blue curve with $B = 0.27$. Notably, to our knowledge, this should be the first holographic example that yields non-monotonic temperature dependence of η_{\parallel}/s in the context of Einstein gravity⁸. More interestingly, when B is relatively large, *i.e.* $B > 0.312$, the non-monotonic behavior in η_{\parallel}/s persists, but it develops two local minima, see *e.g.* the yellow curve with $B = 0.316$. In this case, as the temperature drops, η_{\parallel}/s first decreases, then increases, then decreases again, and finally increases (see the top-right panel for more details). However, the non-monotonicity disappears for a sufficiently strong magnetic field above a special value $B_t \approx 0.975B_c \approx 0.324$. For $B \in (B_t, B_c)$, η_{\parallel}/s decreases monotonically to a small but finite value as the temperature drops, see *e.g.* the purple curve with $B = 0.33$ (also shown in an enlarged version in the bottom-right panel of

⁷Although a good order parameter is absent at finite temperatures, one could identify an order parameter at zero temperature limit. For example, in the classical J-current model, the squared winding numbers serve as the order parameter and are adopted to identify the QCP through their scaling behavior near the QPT [69].

⁸For a discussion on the temperature dependence of the shear viscosity to entropy ratio in the presence of higher derivative corrections, see [51, 52].

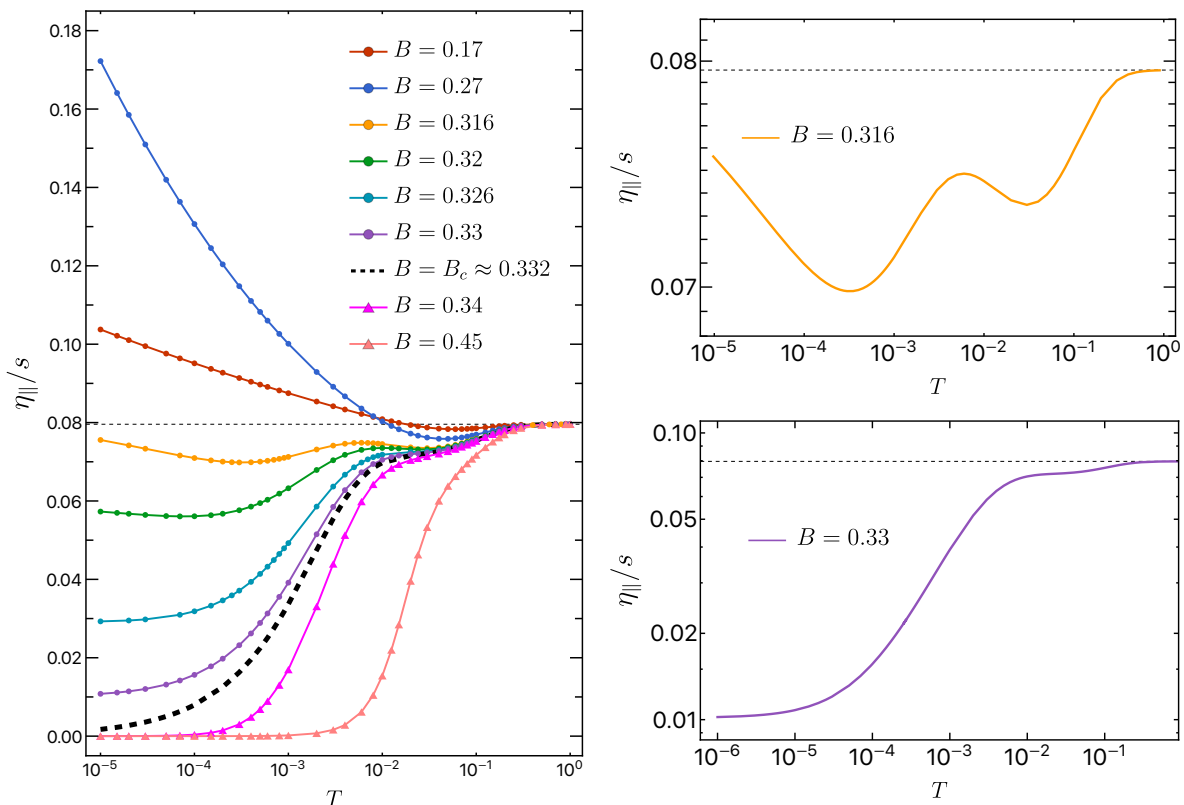


Figure 4: Left panel: The ratio $\eta_{||}/s$ as a function of temperature for selected values of B . Right panel: $\eta_{||}/s$ versus temperature at $B = B_c$ (top-right) and $B = 0.33$ (bottom-right). The dashed horizontal line represents the KSS value $\eta/s = \frac{1}{4\pi}$. The plots are generated for $k = 2/\sqrt{3}$ and $\mu = 1$.

Figure 4). For $B > B_c$, it vanishes at zero temperature following a power law $\sim T^2$, as demonstrated in the right panel of Figure 3.

Of particular interest is the scaling behavior of $\eta_{||}/s$ at B_c . As shown in Figure 5, the ratio $\eta_{||}/s$ scales as

$$\eta_{||}/s \propto T^{2/3}, \quad (3.11)$$

which is in sharp contrast to the quadratic scaling when $B > B_c$. The exponent $2/3$ herein can be understood as a direct combination of the dynamical critical exponent $z = 3$ and the correlation length exponent $\nu = 1/2$ of the QCP, *i.e.* $2/3 = 1/(z\nu)$, see (2.7). Moreover, the deviation from the scaling law (3.11) as increasing the temperature suggests that the quantum critical regime develops well below $T \sim 10^{-3}$. Nevertheless, the non-monotonic behavior of $\eta_{||}/s$ versus T for $B < B_t$ typically happens at temperatures higher than $T \sim 10^{-3}$ (see the left panel of Figure 4). Moreover, the non-monotonic behavior of Figure 4 disappears by turning off the CS coupling, see Appendix C.

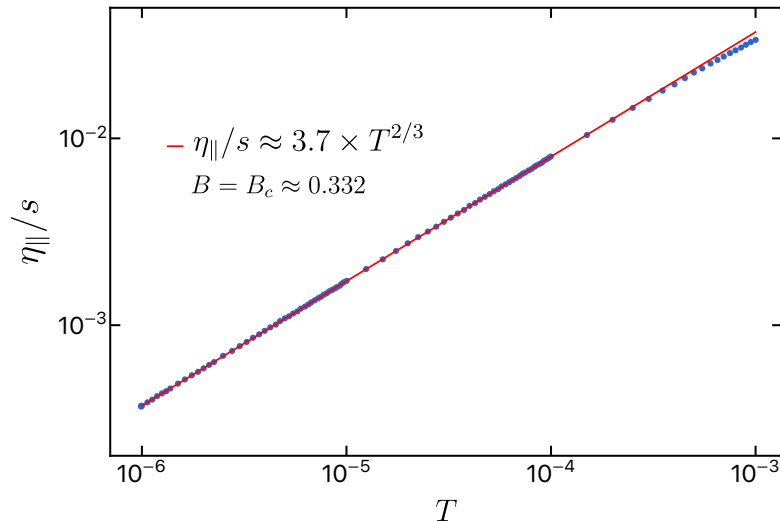


Figure 5: Temperature dependence of $\eta_{||}/s$ at B_c . The red solid curve is obtained by fitting low temperature data (denoted by blue dots). We have set $k = 2/\sqrt{3}$ and $\mu = 1$.

4 Butterfly velocity

In this section, we study the butterfly velocity using shock wave analysis as well as the phenomenon of pole-skipping. Our primary interest here is to carefully investigate the behavior of the butterfly velocity during QPT and to explore its relationship with the shear viscosity studied in the previous section.

4.1 Butterfly velocity from shock wave geometry

The sensitivity to initial conditions or chaos of the boundary field theory could be studied holographically through shock wave solutions [58]. To study the shock wave on an eternal black hole background, it is more convenient to work with the smooth Kruskal coordinates U and V , following [25, 59]. More precisely, we consider the following coordinate transformation:

$$\begin{cases} t - r^* = \hat{v} \\ t + r^* = \hat{u} \end{cases} \implies \begin{cases} V = e^{-\frac{f'(r_h)}{2}\hat{v}} \\ U = -e^{\frac{f'(r_h)}{2}\hat{u}} \end{cases} \quad (4.1)$$

with $UV = -e^{f'(r_h)r^*}$, $U/V = -e^{f'(r_h)t}$ and $dr^* = \frac{dr}{\sqrt{f(f-h^2p^2)}}$ the tortoise coordinate. The background ansatz (2.4) is then rewritten as

$$ds^2 = \frac{1}{r^2} \left[-C dU dV + g(dx^2 + dy^2) + h^2 dz^2 + \frac{2ph^2}{f'(r_h)} \left(\frac{dU}{U} - \frac{dV}{V} \right) dz \right], \quad (4.2)$$

$$A = \frac{A_t}{f'(r_h)} \left(\frac{dU}{U} - \frac{dV}{V} \right) - \frac{B}{2} y dx + \frac{B}{2} x dy - A_z dz,$$

where $C(U, V) = \frac{4(f-h^2p^2)}{f'(r_h)^2} e^{-f'(r_h)r^*}$.

Consider a few particles falling into the black hole from the left boundary of the eternal black hole. The effect of the perturbation is negligible if the particles are released at a small t_w in the past. However, if t_w becomes sufficiently large, the particle's energy, when measured at the $t = 0$ slice, will grow exponentially, resulting in a significant backreaction on the background geometry. The shock wave geometry produced by these perturbations is described by (4.2) for $U > 0$ and by (4.2) with a shift along V direction $V \rightarrow V + H(\vec{x})$ for $U < 0$. After a redefinition of V coordinate, the shock wave configuration is given by

$$ds^2 = -\frac{C}{r^2} dU dV + \frac{g}{r^2} (dx^2 + dy^2) + \frac{h^2}{r^2} dz^2 + \frac{2ph^2}{f'(r_h)r^2} \left(\frac{dU}{U} - \frac{dV}{V} \right) dz$$

$$+ \frac{C}{r^2} H(\vec{x}) \delta(U) dU^2 + \frac{2ph^2}{f'(r_h)r^2 V} H(\vec{x}) \delta(U) dU dz, \quad (4.3)$$

$$A = \frac{A_t}{f'(r_h)} \left(\frac{dU}{U} - \frac{dV}{V} \right) - \frac{B}{2} y dx + \frac{B}{2} x dy - A_z dz + \frac{A_t}{f'(r_h)V} H(\vec{x}) \delta(U) dU.$$

The above geometry is uniquely characterized by the magnitude $H(\vec{x})$, which can be determined by the UU -component of the Einstein equation. Plugging the above ansatz into the Einstein and Maxwell equations and using the fact $U\delta'(U) = -\delta(U)$ and $U\delta(U) = 0$, we derive the (shock wave) equation for $H(\vec{x})$ as

$$\left[-\partial_x^2 - \partial_y^2 - \frac{g}{h^2} \partial_z^2 - gp' \partial_z + m_0^2 \right] H(\vec{x}) \propto \frac{16\pi G_N E_0 g}{C} e^{2\pi T t_w} \delta(\vec{x}), \quad (4.4)$$

where $m_0^2 = \frac{g}{4} (24 - A_t^2 - h^2 p^2) - \frac{B^2}{4g}$ and all the background fields herein are evaluated at the event horizon. Note that E_0 and t_w represent the initial energy and time of the particles, respectively. Unlike the situations in static black holes, there is a linear derivative term ∂_z presented in (4.4), resulting in the splitting of butterfly velocities in the direction \vec{z} , as will be shown later.

To solve (4.4), it is convenient to express $H(\vec{x})$ in momentum space as

$$H(\vec{x}) = \int_{-\infty}^{+\infty} H_0 e^{ik^i x_i} d^3 k_i. \quad (4.5)$$

By substituting (4.5) into (4.4), H can be computed using contour integration. Especially, for the case where \vec{k} is perpendicular to \vec{B} , the solution is given by

$$H(x_\perp) = \int_{-\infty}^{+\infty} e^{ikx_\perp} \frac{e^{2\pi T t_w} E_0}{k^2 - m_0^2} dk \sim \frac{\pi E_0}{m_0} e^{2\pi T(t_w - t_*) - m_0|x|}. \quad (4.6)$$

Here, $t_* = \frac{1}{2\pi T} \ln\left(\frac{c_0}{G}\right) \approx \frac{\ln N^2}{2\pi T}$ with c_0 a constant. Compared to (1.1), the butterfly velocity along the transverse direction reads

$$v_B^\perp = \frac{2\pi T}{m_0}. \quad (4.7)$$

On the other hand, for the case where \vec{k} is parallel to \vec{B} , the solution of H is

$$\begin{aligned} H(z) &= \int_{-\infty}^{+\infty} e^{ikz} \frac{h^2}{g} \frac{e^{2\pi T t_w} E_0}{k^2 + i\frac{h^2 p'}{f} k - \frac{h^2}{g} m_0^2} dk \\ &\sim \begin{cases} \frac{2\pi h E_0}{g\sqrt{24 - A_t^2 - B^2/g^2}} e^{2\pi T(t_w - t_*) - k_+ z}, & z > 0 \\ \frac{2\pi h E_0}{g\sqrt{24 - A_t^2 - B^2/g^2}} e^{2\pi T(t_w - t_*) - k_- |z|}, & z < 0 \end{cases} \end{aligned} \quad (4.8)$$

where $k_\pm = \frac{h_0}{2} (h_0 p_0 \pm \sqrt{24 - A_{t_0}^2 - B^2/g_0^2})$. Therefore, we have two butterfly velocities in the direction $\vec{k} \parallel \vec{B}$, with

$$v_{B\pm}^\parallel = \frac{2\pi T}{k_\pm}, \quad (4.9)$$

where \pm symbols represent the information spreading parallel and antiparallel to the magnetic field direction, respectively.

The key result of (4.9) is that there exist two distinct butterfly velocities when measured in a direction parallel to the magnetic field, as first found in [25] for $\mu \ll T$ and $B \ll T^2$. Additionally, the splitting of longitudinal butterfly velocities supports the idea that chiral anomaly can be macroscopically manifested through the lens of quantum chaos [25, 26]. Similar splitting of butterfly velocity also exist in rotating black holes *e.g.* Kerr-AdS₄ and Myers-Perry-AdS₅ black hole, which are understood as perturbations “upstream” and “downstream” against the direction of rotation [70, 71]. Remarkably, the same expressions for butterfly velocity (4.7) and (4.9) can be extracted by studying the pole-skipping phenomenon [63]. In order to verify the above results obtained from the shock wave analysis, we will also calculate the butterfly velocity by studying the energy density dynamics of the system.

4.2 Butterfly velocity from pole-skipping

To study the pole-skipping phenomenon, we should consider the near horizon perturbations with ingoing boundary conditions. One elegant way to impose the ingoing boundary

condition at the black hole horizon is to work with the Eddington-Finkelstein coordinates. The coordinates transformation are

$$dv = dt - \frac{dr}{f}, \quad d\tilde{z} = dz + \frac{p}{f}dr, \quad (4.10)$$

and the corresponding background becomes⁹

$$ds^2 = \frac{1}{r^2} \left[- (f - h^2 p^2) dv^2 - 2dvdr + 2ph^2 dv d\tilde{z} + g(dx^2 + dy^2) + h^2 d\tilde{z}^2 \right], \quad (4.11)$$

$$A = A_t dv - \frac{B}{2} y dx + \frac{B}{2} x dy - A_z d\tilde{z},$$

where we have used the gauge symmetry to set $A_r = -\frac{A_t + pA_z}{f}$ in (4.11) to zero.

Consider the energy density perturbation $\delta g_{vv}(r, v, x_i) = \delta g_{vv}(r) e^{-i\omega v + ik_i x^i}$ together with other perturbations that couple with it. At the black hole event horizon, the equation of δg_{vv} takes

$$\left[gk_{\parallel}^2 + h^2 k_{\perp}^2 + ik_{\parallel} g h^2 p' + \frac{Br^2 h^2}{2g} + \frac{gh^2}{2r^2} (r^4 A_t'^2 + r^2 h^2 p'^2 - 24) \right. \\ \left. + \frac{(i\omega + f')h}{r} (rg'h + rgh' - 3gh) \right] \delta g_{vv} \quad (4.12)$$

$$+ \left(\omega + \frac{if'}{2} \right) \left[2(k_{\parallel} g \delta g_{v\parallel} + k_{\perp} h^2 \delta g_{v\perp}) + \omega (g \delta g_{zz} + h^2 \delta g_{xx} + h^2 \delta g_{yy}) \right] \Big|_{r=r_h} = 0.$$

Therefore, δg_{vv} decouples from other perturbations at $\omega = \omega_p = -\frac{if'}{2}|_{r_h} = i2\pi T$. Moreover, the pole-skipping point is defined as the special point ($\omega = \omega_p, k = k_p$) for which the coefficient of δg_{vv} is equal to zero and thus the above equation holds automatically [63]. The butterfly velocity is then given by $v_B = \omega_p/k_p$. For $\vec{k} \perp \vec{B}$, we obtain the butterfly velocity

$$v_B^{\perp} = \frac{4\pi T}{\sqrt{g_0(24 - A_{t0}^2 - h_0^2 p_0^2) - B^2/g_0}}. \quad (4.13)$$

On the other hand, for $\vec{k} \parallel \vec{B}$, the butterfly velocity reads

$$v_{B\pm}^{\parallel} = \frac{4\pi T}{p_0 h_0^2 \pm h_0 \sqrt{24 - A_{t0}^2 - B^2/g_0^2}}, \quad (4.14)$$

⁹Strictly speaking, the ingoing null coordinate should be \hat{v} with $d\hat{v} = dt - \frac{dr}{\sqrt{f(f-h^2p^2)}}$. However, as one approaches the black hole horizon, the v coordinate becomes null coordinate and thus is equal to \hat{v} at the leading order in $(r_h - r)$. Therefore, the ingoing mode corresponds to $e^{-i\omega v} \simeq e^{-i\omega \left(t + \frac{\ln(r_h - r)}{4\pi T} \right)} = e^{-i\omega t} (r_h - r)^{-\frac{i\omega}{4\pi T}} \propto e^{-i\omega t} f^{-\frac{i\omega}{4\pi T}}$. The coordinates (4.11) have also been used in the study of quasi-normal modes of this model [23].

where \pm denote the information spreading along $+\vec{B}$ or $-\vec{B}$ direction, respectively. The expressions (4.13) and (4.14) derived from pole skipping are in complete agreement with the results (4.7) and (4.9) from shock wave analysis.

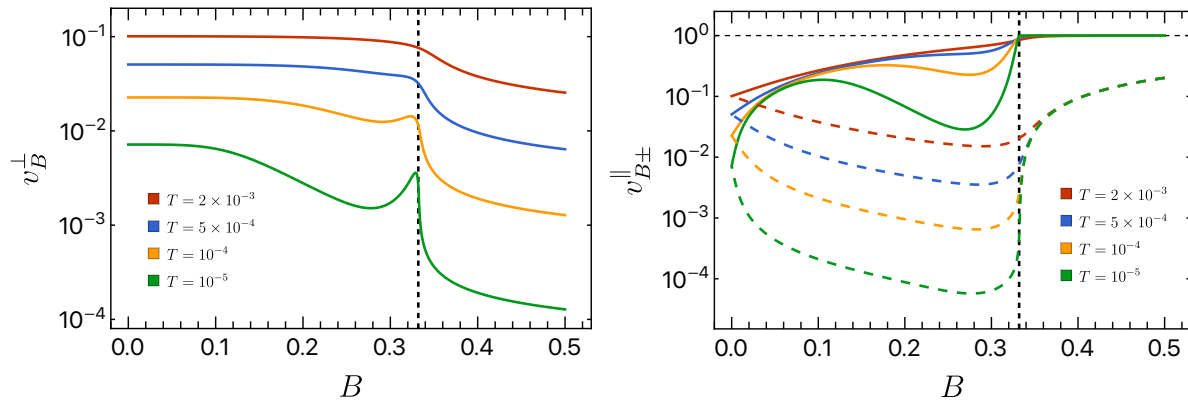


Figure 6: The three butterfly velocities ($v_B^\perp, v_{B\pm}^\parallel$) as a function of magnetic field at different temperatures. In the right panel, the solid lines represent the butterfly velocity v_{B+}^\parallel while the dashed lines represent v_{B-}^\parallel . The location of B_c is denoted by the dashed vertical line. The plots are generated for $k = 2/\sqrt{3}$ and $\mu = 1$.

Figure 6 shows the behavior of butterfly velocities as a function of background magnetic field at different temperatures. As the temperature drops, one finds that the overall amplitude of the transverse butterfly velocity v_B^\perp (left panel) decreases, meanwhile a local maximum develops at B_c for sufficiently low temperatures. On the other hand, the longitudinal butterfly velocities (right panel) always split into v_{B+}^\parallel and v_{B-}^\parallel and satisfy $v_{B+}^\parallel > v_{B-}^\parallel$, which was first found in [25, 26]. Above B_c , v_{B+}^\parallel is always equal to 1 and the difference between v_{B+}^\parallel and v_{B-}^\parallel becomes small by increasing B . In contrast, non-monotonic features are shown when $B < B_c$ at low temperatures. Particularly, approaching the limit $T \rightarrow 0$, one has $v_{B+}^\parallel = 1$ and $v_{B-}^\parallel = 0$ at B_c .

The properties of longitudinal butterfly velocities $v_{B\pm}^\parallel$ have been suggested as an indicator of the QPT in [26]. Nevertheless, in order to precisely locate the QCP, it is necessary to have two butterfly velocities readily available. Here, we demonstrate that each butterfly velocity can independently serve as indicators of the QPT, thanks to their abrupt changes in the vicinity of the QCP. More precisely, we focus on the derivative of the butterfly velocity with respect to B , which indicates the sensitivity of the butterfly velocity against the change in magnetic field. In Figure 7, it is easy to see that $\partial v_B / \partial B$ shows a dip (left), a peak (middle) or a jump (right) as approaching the QCP. The drastic changes become more and more pronounced as we approach the QCP. On the other hand, thermal effects smooth out these changes, suggesting that $\partial v_B / \partial B$ might be good probes

not only for the QCP but also for the quantum critical region.¹⁰

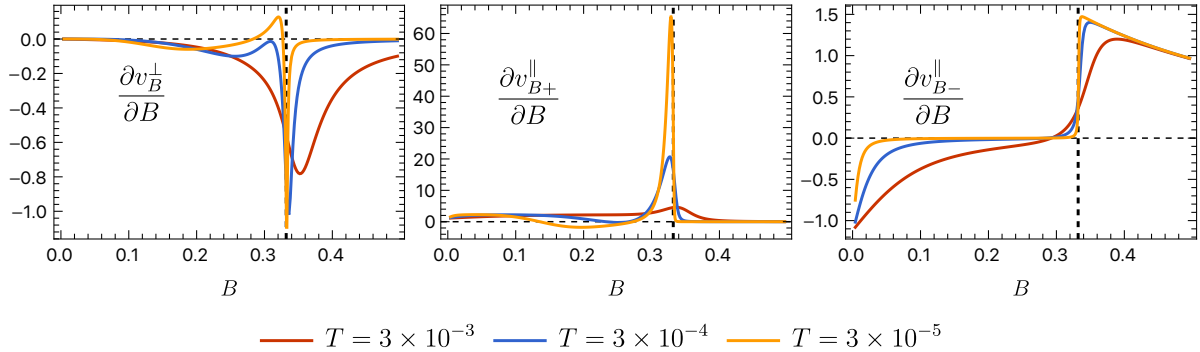


Figure 7: The derivative of butterfly velocities with respect to B for different values of temperature. The vertical dashed line indicates the location of the QCP. Sudden changes are obvious near the QCP. We consider $k = 2/\sqrt{3}$ and $\mu = 1$.

4.3 Relation between shear viscosity and butterfly velocity

Before ending this section, we consider the relation between shear viscosity and butterfly velocity. For many anisotropic but static systems, the butterfly velocities are related to the value of metric functions at the horizon. For a 5-dimensional static metric with anisotropy in the z direction, the horizon formula reads [53]¹¹

$$\frac{(v_B^\parallel)^2}{(v_B^\perp)^2} = \frac{g_{xx}}{g_{zz}} \Big|_{r \rightarrow r_h}. \quad (4.15)$$

Meanwhile, the shear viscosities satisfy

$$\frac{\eta_\parallel}{\eta_\perp} = \left(\frac{g_{xx}}{g_{zz}} \right)^\mathcal{P} \Big|_{r \rightarrow r_h}, \quad (4.16)$$

where $\eta_\perp/s = \frac{1}{4\pi}$. The exponent $\mathcal{P} = -1$ if the anisotropy is induced by the magnetic field [41] and $\mathcal{P} = 1$ if the anisotropy is triggered by other fields, *e.g.* axion field [38] and vector hair [46]. This observation motivates us to conjecture a universal relation between shear viscosity and butterfly velocity, *i.e.*

$$\frac{\eta_\parallel}{s} \left(\frac{(v_B^\perp)^2}{(v_B^\parallel)^2} \right)^\mathcal{P} = \frac{1}{4\pi} \quad (4.17)$$

¹⁰Similar idea has been explored in holographic model with metal-insulator transition [72].

¹¹Note that for static case, there is no splitting of longitudinal butterfly velocities.

This could serve as a novel bound for the shear viscosity to entropy ratio, generalizing the KSS bound to anisotropic systems. In particular, obtaining an expression for the butterfly velocity is relatively straightforward. In fact, this bound is valid in various anisotropic systems with different matter contents, including [41–46].

The model studied in this paper is anisotropic due to the presence of magnetic field, which motivates us to explore such a relationship within our model and subsequently derive an expression for the ratio η_{\parallel}/s . However, we numerically check that the new bound (4.17) does not hold in the present case. The key difference compared to previous anisotropic models is that the bulk geometry of the EMCS model is stationary because of the non-trivial contribution from the CS coupling. In fact, the stationary properties and the quantum anomaly inherent in the system have resulted in the splitting of butterfly velocities in the direction parallel to the magnetic field and thus increase the difficulty in constructing such a bound.

Nonetheless, we numerically check the temperature dependence of the butterfly velocities at $B = B_c$ and find that

$$v_B^{\perp} \propto T^{\alpha}, \quad v_{B-}^{\parallel} \propto T^{\alpha}, \quad 1 - v_{B+}^{\parallel} \propto T^{\beta}, \quad (4.18)$$

where $\alpha = 0.666 \approx 2/3$ and $\beta = 0.469$. This implies that the temperature scaling of v_B^{\perp} or v_{B-}^{\parallel} has the same exponent as that of the ratio η_{\parallel}/s above the QCP. Although (4.17) is violated for the stationary case, it is possible to obtain a new bound for the stationary case by generalizing (4.17) with an appropriate combination of longitudinal and transverse butterfly velocities, *e.g.*

$$\frac{\eta_{\parallel}}{s} \left(\frac{(v_B^{\perp})^2}{\mathcal{F}(v_{B+}^{\parallel}, v_{B-}^{\parallel})^2} \right)^{\mathcal{P}} = \frac{1}{4\pi}, \quad (4.19)$$

where \mathcal{F} is defined as a function of v_{B+}^{\parallel} and v_{B-}^{\parallel} . For the static case where $v_{B+}^{\parallel} = v_{B-}^{\parallel} = v_B^{\parallel}$, we should have $\mathcal{F} = v_B^{\parallel}$ and (4.19) recovers (4.17).

5 Conclusion and discussion

We have studied the shear viscosity and butterfly velocity in a class of strongly coupled quantum many body systems holographically dual to the EMCS theory, which allows a magnetic field driven QPT with the QCP at B_c . Our work is a natural continuation of [16, 25, 26] which initiated this line of research. Since no symmetry is broken in this QPT, there exists no conventional order parameter. Nevertheless, from the bulk point of view, it can be considered as a transition from a “fractionalized” phase with charged horizons ($B < B_c$) to a “cohesive” phase with charged matter ($B > B_c$).

In addition to confirming previous results in the literature, we have uncovered some interesting and novel features. First, we found that the longitudinal shear viscosity-entropy ratio η_{\parallel}/s versus temperature shows a very rich behavior, depending on the value of B , see Figure 4. For a relatively small magnetic field, η_{\parallel}/s initially decreases as the temperature is lowered and rises to a value much larger than the KSS bound. This creates a minimum for η_{\parallel}/s at an intermediate temperature, which resembles the minimum observed in the liquid-gas transition. This is the first explicit example that yields non-monotonic temperature dependence of η/s in Einstein gravity. Although the reason for such a minimum is still unclear, we note that this non-monotonic feature develops at relatively high temperatures and thus might be not closely related to the ground state geometry and the QCP. Even more interesting is the fact that the QPT is visible in the low-temperature behavior of the shear viscosity. Upon approaching QCP, η_{\parallel}/s is finite for $B < B_c$ and vanishes for $B > B_c$. Therefore, the value of η_{\parallel}/s can serve as the order parameter that distinguishes the two states of the system and identifies the QCP through their low temperature behaviors. What's more, we elaborated further on the fact that the splitting of longitudinal butterfly velocities at $T \rightarrow 0$ encodes important information about the QCP. More interestingly, we have uncovered that not only the longitudinal butterfly velocities but also the transverse butterfly can be used to identify the location of QCP. As shown in Figure 7, all the butterfly velocities undergo rapid changes near the QCP, rendering the peak or singularity in their derivatives $\partial v_B/\partial B$ as reliable indicators of the QCP. We also discuss the possible relationship between shear viscosity and butterfly velocity.

There are many interesting questions that could be explored in future work. First, it would be interesting to derive an analytical expression for η_{\parallel}/s , perhaps by adopting the method outlined in [73, 74] or through some variation of the method used in [43, 46]. This endeavor will not only deepen our understanding of the non-trivial behavior of η_{\parallel}/s but will also be invaluable in exploring the relationship between shear viscosity and other transport coefficients [53]. Second, we have limited ourselves to the holographic field theory with the supersymmetric value of the CS coupling. It would be interesting to study the shear viscosity and butterfly velocity for other values of CS coupling k , testing the universality of our findings. Third, we anticipate analogous non-monotonic temperature dependence of the shear viscosity to entropy ratio to emerge in other cases. For example, in holographic Weyl semimetals with momentum relaxation [75, 76], the interplay between spontaneous symmetry breaking driven by a sourceless scalar field and anisotropy induced by the axial $U(1)$ gauge field could potentially give rise to a minimum in η/s . Moreover, the critical theory in our present study is effectively 1+1 dimensional, because massless propagation at the critical point takes place along a single spatial direction. It is also interesting to study quantum criticality in higher dimensions. In particular, the case of 2+1 dimensions is relevant to various layered materials such as

cuprates. Finally, it is of significance to test our results with some experimental setups.

Acknowledgments

We thank Tan Chen, Hao-Tian Sun and Wei-Jia Li for useful discussions. This work was partly supported by the National Natural Science Foundation of China Grants No. 12075298, No. 12122513, No. 12247156, and No. 12047503. We acknowledge the use of the High Performance Cluster at the Institute of Theoretical Physics, Chinese Academy of Sciences.

A Holographic renormalization

Close to the conformal boundary $r \rightarrow 0$, the metric and gauge field take the following form:

$$\begin{aligned}
f(r) &= 1 + 2\xi r + \xi^2 r^2 + \frac{B^2}{6} r^4 \ln r + f_4 r^4 + \dots, \\
g(r) &= 1 + 2\xi r + \xi^2 r^2 - \frac{B^2}{12} r^4 \ln r - h_4 r^4 + \dots, \\
h(r) &= 1 + \xi r + \frac{B^2}{12} r^4 \ln r + h_4 r^4 + \dots, \\
p(r) &= p_4 r^4 - 4p_4 \xi r^5 + \dots, \\
A_t(r) &= \mu - \frac{\rho}{2} r^2 + \xi \rho r^3 + \dots, \\
A_z(r) &= A_{z2} r^2 - 2\xi A_{z2} r^3 + \dots.
\end{aligned} \tag{A.1}$$

Note that, the constant ξ reflects the reparameterization freedom $r \rightarrow r + \xi$ along the radial direction and can be set to zero. Near the event horizon $r = r_h$, the bulk fields behave as

$$\begin{aligned}
f(r) &= (r_h - r)f_0 + \dots, & g(r) &= g_0 + \dots, & h(r) &= h_0 + \dots, \\
p(r) &= (r_h - r)p_0 + \dots, & A_t(r) &= (r_h - r)A_{t0} + \dots, & A_z(r) &= A_{z0} + \dots.
\end{aligned} \tag{A.2}$$

Using the scaling symmetry

$$(t, x, y, z, r) \rightarrow c(t, x, y, z, r), \quad (A_t, A_z) \rightarrow c^{-1}(A_t, A_z), \quad B \rightarrow c^{-2}B, \quad (f, g, h, p) \rightarrow (f, g, h, p),$$

we can fix the location of the event horizon $r_h = 1$.

Moreover, the UV expansion for the helicity one perturbations (3.6) reads

$$\begin{aligned}
h_z^x &= h_{xz}^{(0)} + \frac{\omega^2 h_{xz}^{(0)}}{4} r^2 + h_{xz}^{(1)} r^4 + \left(\frac{B^2}{4} - \frac{\omega^4}{16} \right) h_{xz}^{(0)} r^4 \ln r + \dots, \\
h_z^y &= h_{yz}^{(0)} + \frac{\omega^2 h_{yz}^{(0)}}{4} r^2 + h_{yz}^{(1)} r^4 + \left(\frac{B^2}{4} - \frac{\omega^4}{16} \right) h_{yz}^{(0)} r^4 \ln r + \dots, \\
h_t^x &= h_{tx}^{(0)} + h_{tx}^{(1)} r^4 + \left(\frac{B^2 h_{tx}^{(0)}}{4} + \frac{i\omega B a_y^{(0)}}{4} \right) r^4 \ln r + \dots, \\
h_t^y &= h_{ty}^{(0)} + h_{ty}^{(1)} r^4 + \left(\frac{B^2 h_{ty}^{(0)}}{4} - \frac{i\omega B a_x^{(0)}}{4} \right) r^4 \ln r + \dots, \\
a_x &= a_x^{(0)} + a_x^{(1)} r^2 - \left(\frac{\omega^2 a_x^{(0)}}{2} + \frac{i\omega B h_{ty}^{(0)}}{2} \right) r^2 \ln r + \dots, \\
a_y &= a_y^{(0)} + a_y^{(1)} r^2 - \left(\frac{\omega^2 a_y^{(0)}}{2} - \frac{i\omega B h_{tx}^{(0)}}{2} \right) r^2 \ln r + \dots,
\end{aligned} \tag{A.3}$$

where $h_{tx}^{(1)}$ and $h_{ty}^{(1)}$ are determined by $a_x^{(1)}$, $a_y^{(1)}$ as well as the leading order source terms.

The renormalised on-shell action is given by

$$S_{ren} = S + S_{bdy} \tag{A.4}$$

where

$$S_{bdy} = \frac{1}{16\pi G} \int d^4x \sqrt{-\gamma} \left[2K - \frac{6}{L} - \frac{L\hat{R}}{2} + \frac{L}{4} \ln\left(\frac{r}{L}\right) \left(\hat{R}_{\mu\nu} \hat{R}^{\mu\nu} - \frac{\hat{R}^2}{3} - F^2 \right) \right].$$

Here $\gamma_{\mu\nu}$ is the induced metric at the conformal boundary, K is the trace of extrinsic curvature and $\hat{R}_{\mu\nu}$ denotes the Ricci tensor associated with $\gamma_{\mu\nu}$.

The stress tensor and current of the dual field theory are

$$\begin{aligned}
\langle T_{\mu\nu} \rangle &= \lim_{r \rightarrow 0} \frac{1}{r^2} \left[-2K_{\mu\nu} + 2(K-3)\gamma_{\mu\nu} + \hat{G}_{\mu\nu} + \ln r (F_{\mu\rho} F_{\nu}{}^\rho - \frac{\gamma_{\mu\nu}}{4} F^2 - h_{\mu\nu}^{(4)}) \right], \\
\langle J^\mu \rangle &= \lim_{r \rightarrow 0} \sqrt{-\gamma} \left[n_r \left(F^{\mu r} + \frac{k}{6} \epsilon^{r\mu\alpha\beta\gamma} A_\alpha F_{\beta\gamma} \right) + \nabla_\alpha F^{\alpha\mu} \ln r \right],
\end{aligned} \tag{A.5}$$

with $h_{\mu\nu}^{(4)} = \hat{R}_{\mu\rho\nu\lambda} \hat{R}^{\rho\lambda} - \frac{1}{6} \hat{\nabla}_\mu \hat{\nabla}_\nu \hat{R} + \frac{1}{2} \hat{\nabla}^2 \hat{R}_{\mu\nu} - \frac{1}{3} \hat{R} \hat{R}_{\mu\nu} - \frac{\gamma_{\mu\nu}}{4} (\hat{R}_{\rho\lambda} \hat{R}^{\rho\lambda} - \frac{\hat{R}^2}{3} + \frac{\hat{\nabla}^2 \hat{R}}{3})$.

Therefore, the non-zero components of the stress tensor $\langle T_{\mu\nu} \rangle$ are

$$\begin{aligned}
\epsilon = \langle T_{tt} \rangle &= -3f_4, & \mathcal{P}_\perp = \langle T_{xx} \rangle = \langle T_{yy} \rangle &= -\frac{B^2}{4} - f_4 - 4h_4, \\
\mathcal{P}_\parallel = \langle T_{zz} \rangle &= -f_4 + 8h_4, & \langle T_{tz} \rangle = \langle T_{zt} \rangle &= 4p_4 = -\frac{k}{2}B\mu^2, \\
\langle T_{tx} \rangle &= \rho a_x^{(0)} + \frac{i\omega B a_y^{(0)}}{2} + \left(\frac{B^2}{4} - f_4 - 4h_4\right)h_{tx}^{(0)} - \frac{2iB}{\omega} \left(a_y^{(1)} - \frac{\rho h_{ty}^{(0)}}{2} + A_{z2}h_{yz}^{(0)}\right), \\
\langle T_{ty} \rangle &= \rho a_y^{(0)} - \frac{i\omega B a_x^{(0)}}{2} + \left(\frac{B^2}{4} - f_4 - 4h_4\right)h_{ty}^{(0)} + \frac{2iB}{\omega} \left(a_x^{(1)} - \frac{\rho h_{tx}^{(0)}}{2} + A_{z2}h_{xz}^{(0)}\right), \\
\langle T_{xz} \rangle &= 4h_{xz}^{(1)} - h_{xz}^{(0)} \left(\frac{3\omega^4}{16} + f_4 + 4h_4\right), & \langle T_{yz} \rangle &= 4h_{yz}^{(1)} - h_{yz}^{(0)} \left(\frac{3\omega^4}{16} + f_4 + 4h_4\right),
\end{aligned} \tag{A.6}$$

while the non-zero components of the dual current $\langle J_\mu \rangle$ are

$$\begin{aligned}
\langle J_t \rangle &= -\rho, & \langle J_z \rangle &= -2A_{z2} = kB\mu, \\
\langle J_x \rangle &= 2a_x^{(1)} - 2kB\mu h_{xz}^{(0)} - \frac{\omega}{2}(\omega a_x^{(0)} + iBh_{ty}^{(0)}), \\
\langle J_y \rangle &= 2a_y^{(1)} - 2kB\mu h_{yz}^{(0)} - \frac{\omega}{2}(\omega a_y^{(0)} - iBh_{tx}^{(0)}).
\end{aligned} \tag{A.7}$$

where the covariant current is considered by dropping the contribution of the Chern-Simons term.

The free energy density w can be derived from the Euclidean on-shell action, known as the *quantum statistical relation*. One then obtains that

$$w = \frac{W}{V} = -\frac{S_{ren}}{V} = \epsilon - Ts - \mu \langle J^t \rangle - \frac{kB}{3} \int_0^{r_h} A_t A'_z dr, \tag{A.8}$$

where the last term is from the CS coupling. It has been recently revealed that the above free energy density w does not satisfy the first law of thermodynamics [24], *i.e.*

$$\delta w = -\left(s + \frac{kQ_{cs}}{T}\right) \delta T - \rho \delta \mu - k \delta Q_{cs} - M_B \delta B, \tag{A.9}$$

where

$$\begin{aligned}
Q_{cs} &= \frac{B}{6} \int_0^{r_h} (A'_z A_t - A_z A'_t) dr = \frac{B}{3} \int_0^{r_h} A_t A'_z dr, \\
M_B &= -\left(\int_0^{r_h} \left[\frac{B}{r} \left(\frac{h}{g} - 1\right) + \frac{k}{2}(A_t A'_z - A'_t A_z)\right] dr + B \ln r_h\right).
\end{aligned}$$

This issue can be solved by adding the non-local term Q_{cs} to the free energy [24]:

$$\tilde{w} = w + kQ_{cs} = \epsilon - Ts - \mu \langle J^t \rangle, \tag{A.10}$$

and one recovers the standard form of the first law of thermodynamics

$$\delta \tilde{w} = -s \delta T - \langle J^t \rangle \delta \mu - M_B \delta B, \tag{A.11}$$

where M_B is recognized as the magnetization of the system.

B Transverse shear viscosity

For transverse shear viscosity, we can directly obtain an analytical expression following the method used in [46] (see also [43, 77]). Consider the fluctuation of the helicity two mode, denoted as h_{xy} . Defining $X = g^{xx}h_{xy}$, the equation of motion for X reads

$$X'' + \left(\frac{f'}{f} + \frac{g'}{g} + \frac{h'}{h} - \frac{3}{r} \right) X' + \frac{\omega^2}{f^2} X = 0. \quad (\text{B.1})$$

The UV expansion of X is given by

$$X = X^{(0)} + \frac{\omega^2 X^{(0)}}{4} r^2 + X^{(1)} r^4 - \frac{\omega^4 X^{(0)}}{16} r^4 \ln r + \dots, \quad (\text{B.2})$$

and the corresponding stress tensor reads

$$\langle T_{xy} \rangle = [\langle T_{xx} \rangle + i\omega\eta] X^{(0)} = \left[\langle T_{xx} \rangle + \frac{4X^{(1)}}{X^{(0)}} - \frac{3\omega^4}{16} \right] X^{(0)}. \quad (\text{B.3})$$

We then obtain the shear viscosity

$$\eta_{\perp} = \lim_{\omega \rightarrow 0} \frac{1}{i\omega} \left(\frac{4X^{(1)}}{X^{(0)}} - \frac{3\omega^4}{16} \right) = \lim_{\omega \rightarrow 0} \frac{1}{i\omega} \frac{4X^{(1)}}{X^{(0)}}, \quad (\text{B.4})$$

where $X^{(0)}$ can be normalized to one. Therefore, to obtain η_{\perp} , we only need to know $X^{(1)}$ at leading order in ω , which can be expressed analytically by the horizon data. More precisely, we expand X in powers of ω ,

$$X = f^{-\frac{i\omega}{4\pi T}} (X_0 + \omega X_1 + \dots), \quad (\text{B.5})$$

where the temperature-dependent prefactor is to ensure that the perturbations obey the ingoing boundary conditions at the horizon. The equation (B.1) can be solved order by order in powers of ω . We have

$$X_0 = 1, \quad X_1 = \int_1^r \left(\frac{if'}{4\pi T f} + ig_0 h_0 \frac{\tilde{r}^3}{fgh} \right) d\tilde{r}. \quad (\text{B.6})$$

Note that, X_1 is fixed by regularity condition near the black hole horizon. The near boundary expansion of X at leading order in ω reads

$$X = 1 + \omega c_0 + \frac{i\omega g_0 h_0}{4} r^4 + \dots, \quad (\text{B.7})$$

where $c_0 = \int_1^0 \left(\frac{if'}{4\pi T f} + ig_0 h_0 \frac{\tilde{r}^3}{fgh} \right) d\tilde{r}$ is a constant. Then, we can find that $X^{(0)} = 1 + \omega c_0$ and $X^{(1)} = i\omega g_0 h_0 / 4$ for small ω . Therefore, we get

$$\eta_{\perp} = \lim_{\omega \rightarrow 0} \frac{1}{i\omega} \frac{4X^{(1)}}{X^{(0)}} = \lim_{\omega \rightarrow 0} \frac{1}{i\omega} \frac{i\omega g_0 h_0}{1 + \omega c_0} = g_0 h_0, \quad \Rightarrow \quad \frac{\eta_{\perp}}{s} = \frac{1}{4\pi}. \quad (\text{B.8})$$

C Longitudinal shear viscosity for $k = 0$

To compare with the key results shown in the main text, we present additional results of the ratio of longitudinal shear viscosity to entropy density at zero CS coupling *i.e.* $k = 0$, for which the bulk spacetime (2.4) becomes static with $p = A_z = 0$. As shown in Figure 4, the intriguing non-monotonic temperature dependence of η_{\parallel}/s emerges at small magnetic field in the presence of CS coupling. Consequently, our analysis will focus on the small B regime.

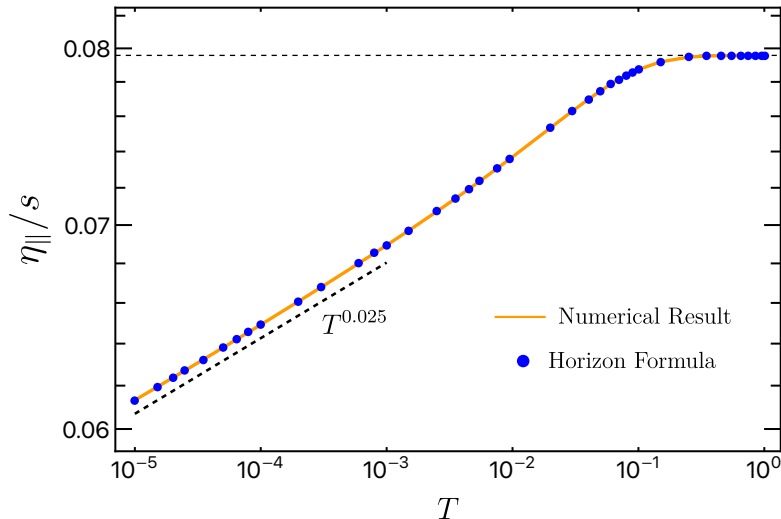


Figure 8: The temperature dependence of η_{\parallel}/s at $B = 0.1$ for the CS coupling $k = 0$. The solid line is from the numerical data and blue dots are from our horizon formula (4.16). The black dashed curve is the low temperature scaling of η_{\parallel}/s obtained by fitting the low temperature data. We have set $\mu = 1$.

Figure 8 shows the behavior of η_{\parallel}/s as a function of temperature at $B = 0.1$. The ratio η_{\parallel}/s decreases monotonically as the temperature decreases, in contrast to the non-monotonic behavior revealed for $k = 2/\sqrt{3}$ demonstrated in Figure 4. As $T \rightarrow 0$, the η_{\parallel}/s vanishes following a power law:

$$\eta_{\parallel}/s \propto T^{0.025}. \quad (\text{C.1})$$

It is worth noting that the temperature scaling exponent observed here differs from that of pure magnetic black branes [41]. This discrepancy may be attributed to the interplay between charge density and magnetic field when B is small. Furthermore, we check the numerical results with the horizon formula (4.16), observing excellent agreement. As demonstrated in Figure 8, the numerical data (displayed with solid line) are in perfect agreement with the horizon formula (4.16), shown with blue dots.

References

- [1] S. Sachdev, *Quantum Phase Transitions*, Cambridge University Press, 2011.
- [2] T. Senthil, A. Vishwanath, L. Balents, S. Sachdev and M. P. A. Fisher, *Deconfined Quantum Critical Points*, *Science* **303** (2004) 5663, 1490-1494 [[arXiv:cond-mat/0311326](#)].
- [3] T. Senthil, *Deconfined quantum critical points: a review*, [[arXiv:2306.12638](#)].
- [4] N. P. Armitage, E. J. Mele and A. Vishwanath, *Weyl and Dirac Semimetals in Three Dimensional Solids*, *Rev.Mod.Phys.* **90** (2018) 1, 015001 [[arXiv:1705.01111](#)].
- [5] M. Baggioli, K. Y. Kim, L. Li and W. J. Li, *Holographic Axion Model: a simple gravitational tool for quantum matter*, *Sci. China Phys. Mech. Astron.* **64**, no.7, 270001 (2021) [[arXiv:2101.01892](#)].
- [6] J. M. Maldacena, *The Large N limit of superconformal field theories and supergravity*, *Adv.Theor.Math.Phys.* **2** (1998) 231-252, [[arXiv:hep-th/9711200](#)].
- [7] J. Zaanen, Y. W. Sun, Y. Liu and K. Schalm, *Holographic Duality in Condensed Matter Physics*, Cambridge University Press, 2015.
- [8] S. A. Hartnoll, A. Lucas and S. Sachdev, *Holographic quantum matter*, [[arXiv:1612.07324](#)].
- [9] H. Liu and J. Sonner, *Holographic systems far from equilibrium: a review*, *Rept. Prog. Phys.* **83**, no.1, 016001 (2019) [[arXiv:arXiv:1810.02367](#)].
- [10] N. Iqbal, H. Liu, M. Mezei and Q. Si, *Quantum phase transitions in holographic models of magnetism and superconductors*, *Phys.Rev.D* **82** (2010) 045002, [[arXiv:1003.0010](#)].
- [11] E. D'Hoker and P. Kraus, *Magnetic Field Induced Quantum Criticality via new Asymptotically AdS₅ Solutions*, *Class. Quant. Grav.* **27** (2010) 215022, [[arXiv:1006.2573](#)].
- [12] S. A. Hartnoll and L. Huijse, *Fractionalization of holographic Fermi surfaces*, *Class.Quant.Grav.* **29** (2012) 194001, [[arXiv:1111.2606](#)].
- [13] A. Donos and S. A. Hartnoll, *Interaction-driven localization in holography*, *Nature Phys.* **9** (2013) 649-655, [[arXiv:1212.2998](#)].
- [14] K. Landsteiner, Y. Liu and Y. W. Sun, *Quantum phase transition between a topological and a trivial semimetal from holography*, *Phys.Rev.Lett.* **116** (2016) 8, 081602, [[arXiv:1511.05505](#)].
- [15] E. Witten, *Anti-de Sitter space and holography*, *Adv.Theor.Math.Phys.* **2** (1998) 253-291, [[arXiv:hep-th/9802150](#)].

- [16] M. Ammon, S. Griener, J. Hernandez, M. Kaminski, R. Koirala, J. Leiber and J. Wu, *Chiral hydrodynamics in strong external magnetic fields*, *JHEP* **04** (2021) 078, [[arXiv:2012.09183](#)].
- [17] M. Rangamani, J. Virrueta and S. Zhou, *Anomalous hydrodynamics effective actions from holography*, *JHEP* **11** (2023) 044, [[arXiv:2306.01055](#)].
- [18] E. D'Hoker and P. Kraus, *Magnetic Brane Solutions in AdS*, *JHEP* **10** (2009) 088, [[arXiv:0908.3875](#)].
- [19] E. D'Hoker and P. Kraus, *Holographic Metamagnetism, Quantum Criticality, and Crossover Behavior*, *JHEP* **05** (2010) 083, [[arXiv:1003.1302](#)].
- [20] E. D'Hoker and P. Kraus, *Quantum Criticality via Magnetic Branes*, *Lect.Notes Phys.* **871** (2013) 469-502, [[arXiv:1208.1925](#)].
- [21] D. Astefanesei, N. Banerjee and S. Dutta, *Moduli and electromagnetic black brane holography*, *JHEP* **02** (2011) 021, [[arXiv:1008.3852](#)].
- [22] M. Ammon, J. Leiber and R. P. Macedo, *Phase diagram of 4D field theories with chiral anomaly from holography*, *JHEP* **03** (2016) 164, [[arXiv:1601.02125](#)].
- [23] M. Ammon, M. Kaminski, R. Koirala, J. Leiber and J. Wu, *Quasinormal modes of charged magnetic black branes & chiral magnetic transport*, *JHEP* **04** (2017) 067, [[arXiv:1701.05565](#)].
- [24] R. G. Cai, L. Li and J. K. Zhao, *Thermodynamics of dyonic black holes in minimal supergravity*, [[arXiv:2410.00717](#)].
- [25] N. Abbasi, J. Tabatabaei, *Quantum chaos, pole-skipping and hydrodynamics in a holographic system with chiral anomaly*, *JHEP* **03** (2020) 050, [[arXiv:1910.13696](#)].
- [26] N. Abbasi and K. Landsteiner, *Pole-skipping as order parameter to probe a quantum critical point*, *JHEP* **09** (2023) 169, [[arXiv:2307.16716](#)].
- [27] P. Kovtun, D. T. Son and A. O. Starinets, *Viscosity in strongly interacting quantum field theories from black hole physics*, *Phys.Rev.Lett.* **94** (2005) 111601, [[arXiv:hep-th/0405231](#)].
- [28] P. Kovtun, D. T. Son and A. O. Starinets, *Holography and hydrodynamics: Diffusion on stretched horizons*, *JHEP* **10** (2003) 064, [[arXiv:hep-th/0309213](#)].
- [29] M. Brigante, H. Liu, R. C. Myers, S. Shenker and S. Yaida, *Viscosity Bound Violation in Higher Derivative Gravity*, *Phys.Rev.D* **77** (2008) 126006, [[arXiv:0712.0805](#)].
- [30] M. Brigante, H. Liu, R. C. Myers, S. Shenker and S. Yaida, *The Viscosity Bound and Causality Violation*, *Phys.Rev.Lett.* **100** (2008) 191601, [[arXiv:0802.3318](#)].
- [31] Y. Kats and P. Petrov, *Effect of curvature squared corrections in AdS on the viscosity of the dual gauge theory*, *JHEP* **01** (2009) 044, [[arXiv:0712.0743](#)].

- [32] R. G. Cai, Z. Y. Nie and Y. W. Sun, *Shear Viscosity from Effective Couplings of Gravitons*, *Phys.Rev.D* **78** (2008) 126007, [[arXiv:0811.1665](#)].
- [33] R. C. Myers, M. F. Paulos and A. Sinha, *Holographic studies of quasi-topological gravity*, *JHEP* **08** (2010) 035, [[arXiv:1004.2055](#)].
- [34] X. H. Feng, H. S. Liu, H. Lü and C. N. Pope, *Black Hole Entropy and Viscosity Bound in Horndeski Gravity*, *JHEP* **11** (2015) 176, [[arXiv:1509.07142](#)].
- [35] Y. L. Wang and X. H. Ge, *Shear Viscosity to Entropy Density Ratio in Higher Derivative Gravity with Momentum Dissipation*, *Phys.Rev.D* **94** (2016) 6, 066007, [[arXiv:1605.07248](#)].
- [36] A. Buchel, *Holographic Gauss-Bonnet transport*, *Phys.Lett.B* **853** (2024) 138666, [[arXiv:2410.10161](#)].
- [37] S. Cremonini, *The Shear Viscosity to Entropy Ratio: A Status Report*, *Mod.Phys.Lett.B* **25** (2011) 1867-1888, [[arXiv:1108.0677](#)].
- [38] A. Rebhan and D. Steineder, *Violation of the Holographic Viscosity Bound in a Strongly Coupled Anisotropic Plasma*, *Phys.Rev.Lett.* **108** (2012) 021601, [[arXiv:1110.6825](#)].
- [39] K. A. Mamo, *Holographic RG flow of the shear viscosity to entropy density ratio in strongly coupled anisotropic plasma*, *JHEP* **10** (2012) 070, [[arXiv:1205.1797](#)].
- [40] S. Jain, N. Kundu, K. Sen, A. Sinha and S. P. Trivedi, *A Strongly Coupled Anisotropic Fluid From Dilaton Driven Holography*, *JHEP* **01** (2015) 005, [[arXiv:1406.4874](#)].
- [41] R. Critelli, S. I. Finazzo, M. Zaniboni and J. Noronha, *Anisotropic shear viscosity of a strongly coupled non-Abelian plasma from magnetic branes*, *Phys.Rev.D* **90** (2014) 6, 066006, [[arXiv:1406.6019](#)].
- [42] S. I. Finazzo, R. Critelli, R. Rougemont and J. Noronha, *Momentum transport in strongly coupled anisotropic plasmas in the presence of strong magnetic fields*, *Phys.Rev.D* **94** (2016) 5, 054020, [[arXiv:1605.06061](#)].
- [43] K. Landsteiner, Y. Liu and Y. W. Sun, *Odd viscosity in the quantum critical region of a holographic Weyl semimetal*, *Phys.Rev.Lett.* **117**(2016) 8, 081604, [[arXiv:1604.01346](#)].
- [44] D. Giataganas, U. Gürsoy, J. F. Pedraza, *Strongly-coupled anisotropic gauge theories and holography*, *Phys.Rev.Lett.* **121** (2018) 12, 121601, [[arXiv:1708.05691](#)].
- [45] U. Gürsoy, M. Järvinen, G. Nijs, J. F. Pedraza, *On the interplay between magnetic field and anisotropy in holographic QCD*, *JHEP* **03** (2021) 180, [[arXiv:2011.09474](#)].
- [46] M. Baggioli, S. Cremonini, L. Early, L. Li and H. T. Sun, *Breaking rotations without violating the KSS viscosity bound*, *JHEP* **07** (2023) 016, [[arXiv:2304.01807](#)].

- [47] J. Erdmenger, P. Kerner and H. Zeller, *Transport in Anisotropic Superfluids: A Holographic Description*, *JHEP* **01** (2012) 059, [[arXiv:1110.0007](#)].
- [48] M. Baggioli, L. Li and H. T. Sun, *Shear Flows in Far-from-Equilibrium Strongly Coupled Fluids*, *Phys.Rev.Lett.* **129** (2022) 1, 011602, [[arXiv:2112.14855](#)].
- [49] M. F. Wondrak, M. Kaminski and M. Bleicher, *Shear transport far from equilibrium via holography*, *Phys. Lett. B* **811**, 135973 (2020) [[arXiv:2002.11730](#)].
- [50] S. Wang, S. He and L. Li, *Shear transport in far-from-equilibrium isotropization of supersymmetric Yang-Mills plasma*, [[arXiv:2411.10706](#)].
- [51] S. Cremonini and P. Szepietowski, *Generating Temperature Flow for eta/s with Higher Derivatives: From Lifshitz to AdS*, *JHEP* **02** (2012) 038, [[arXiv:1111.5623](#)].
- [52] S. Cremonini, U. Gursoy and P. Szepietowski, *On the Temperature Dependence of the Shear Viscosity and Holography*, *JHEP* **08** (2012) 167, [[arXiv:1206.3581](#)].
- [53] M. Blake, *Universal Charge Diffusion and the Butterfly Effect in Holographic Theories*, *Phys.Rev.Lett.* **117** (2016) 9, 091601, [[arXiv:1603.08510](#)].
- [54] Y. Gu, X. L. Qi and D. Stanford, *Local criticality, diffusion and chaos in generalized Sachdev-Ye-Kitaev models*, *JHEP* **05** (2017) 125, [[arXiv:1609.07832](#)].
- [55] R. A. Davison, W. Fu, A. Georges, Y. Gu, K. Jensen and S. Sachdev, *Thermoelectric transport in disordered metals without quasiparticles: The Sachdev-Ye-Kitaev models and holography*, *Phys.Rev.B* **95** (2017) 15, 155131, [[arXiv:1612.00849](#)].
- [56] S. Grozdanov, K. Schalm and V. Scopelliti, *Black hole scrambling from hydrodynamics*, *Phys.Rev.Lett.* **120** (2018) 23, 231601, [[arXiv:1710.00921](#)].
- [57] A. I. Larkin and Y. N. Ovchinnikov, *Quasiclassical Method in the Theory of Superconductivity*, *Sov.Phys.JETP* **28** (1969) 1200.
- [58] S. H. Shenker and D. Stanford, *Black holes and the butterfly effect*, *JHEP* **03** (2014) 067, [[arXiv:1306.0622](#)].
- [59] D. A. Roberts, D. Stanford and L. Susskind, *Localized shocks*, *JHEP* **03** (2015) 051, [[arXiv:1409.8180](#)].
- [60] J. Maldacena, S. H. Shenker and D. Stanford, *A bound on chaos*, *JHEP* **08** (2016) 106, [[arXiv:1503.01409](#)].
- [61] V. Jahnke, *Recent developments in the holographic description of quantum chaos*, *Adv.High Energy Phys.* **2019** (2019) 9632708, [[arXiv:1811.06949](#)].
- [62] M. Blake, H. Lee and H. Liu, *A quantum hydrodynamical description for scrambling and many-body chaos*, *JHEP* **10** (2018) 127, [[arXiv:1801.00010](#)].
- [63] M. Blake, R. A. Davison, S. Grozdanov and H. Liu, *Many-body chaos and energy dynamics in holography*, *JHEP* **10** (2018) 035, [[arXiv:1809.01169](#)].

- [64] A. Buchel and J. T. Liu, *Gauged supergravity from type IIB string theory on $Y^{p,q}$ manifolds*, *Nucl.Phys.B* **771** (2007) 93-112, [[arXiv:hep-th/0608002](#)].
- [65] J. P. Gauntlett, E. O Colgain and O. Varela, *Properties of some conformal field theories with M-theory duals*, *JHEP* **02** (2007) 049, [[arXiv:hep-th/0611219](#)].
- [66] S. Nakamura, H. Ooguri and C.-S. Park, *Gravity Dual of Spatially Modulated Phase*, *Phys.Rev.D* **81** (2010) 044018, [[arXiv:0911.0679](#)].
- [67] A. Donos and J. P. Gauntlett, *Black holes dual to helical current phases*, *Phys.Rev.D* **86** (2012) 064010, [[arXiv:1204.1734](#)].
- [68] S. A. Hartnoll and D. Radicevic, *Holographic order parameter for charge fractionalization*, *Phys.Rev.D* **86** (2012) 066001, [[arXiv:1205.5291](#)].
- [69] K. Chen, L. Liu, Y. Deng, L. Pollet and N. Prokofév, *Universal Conductivity in a Two-Dimensional Superfluid-to-Insulator Quantum Critical System*, *Phys.Rev.Lett.* **112** (2014) 3, 030402, [[arXiv:1309.5635v2](#)].
- [70] M. Blake and R. A. Davison, *Chaos and pole-skipping in rotating black holes*, *JHEP* **01** (2022) 013, [[arXiv:2111.11093](#)].
- [71] M. A. G. Amano, M. Blake, C. Cartwright, M. Kaminski and A. P. Thompson, *Chaos and pole-skipping in a simply spinning plasma*, *JHEP* **02** (2023) 253, [[arXiv:2211.00016](#)].
- [72] Y. Ling, P. Liu and J. P. Wu, *Holographic Butterfly Effect at Quantum Critical Points*, *JHEP* **10** (2017) 025, [[arXiv:1610.02669](#)].
- [73] A. Donos, P. Kailidis and C. Pantelidou, *Holographic dissipation from the symplectic current*, *JHEP* **10** (2022) 058, [[arXiv:2208.05911](#)].
- [74] T. Demircik, D. Gallegos, U. Gürsoy, M. Järvinen and R. Lier, *A novel method for holographic transport*, [[arXiv:2311.00042](#)].
- [75] J. K. Zhao, *Momentum relaxation in a holographic Weyl semimetal*, *Phys.Rev.D* **104** (2021) 6, 066003, [[arXiv:2109.07215](#)].
- [76] J. K. Zhao, *Momentum relaxation of holographic Weyl semimetal from massive gravity*, *Eur.Phys.J.C* **82** (2022) 4, 300, [[arXiv:2111.14068](#)].
- [77] M. Baggioli and A. Buchel, *Holographic Viscoelastic Hydrodynamics*, *JHEP* **03** (2019) 146, [[arXiv:1805.06756](#)].